Journal of Radiation Research, 2014, 55, 1153–1162
doi: 10.1093/jrr/rru056 Advance Access Publication 30 June 2014

Computer-assisted delineation of lung tumor regions in treatment planning CT images with PET/CT image sets based on an optimum contour selection method

Ze JIN[1], Hidetaka ARIMURA[2,*], Yoshiyuki SHIOYAMA[3], Katsumasa NAKAMURA[4], Jumpei KUWAZURU[5], Taiki MAGOME[1], Hidetake YABU-UCHI[2], Hiroshi HONDA[4], Hideki HIRATA[2] and Masayuki SASAKI[2]

[1]Department of Health Sciences, Graduate School of Medical Sciences, Kyushu University, 3-1-1, Maidashi, Higashi-ku, Fukuoka 812–8582, Japan
[2]Department of Health Sciences, Faculty of Medical Sciences, Kyushu University, 3-1-1, Maidashi, Higashi-ku, Fukuoka 812–8582, Japan
[3]Department of Heavy Particle Therapy and Radiation Oncology, Graduate School of Medical Sciences, Kyushu University, Fukuoka, Japan
[4]Department of Clinical Radiology, Graduate School of Medical Sciences, Kyushu University, Fukuoka, Japan
[5]Medipolis Proton Therapy and Research Center, Higashikata, Ibusuki-shi, Kagoshima, Japan
*Corresponding author: Tel and Fax: +81-92-642-6719; Email: arimurah@med.kyushu-u.ac.jp

(Received 20 June 2013; revised 31 May 2014; accepted 3 June 2014)

To assist radiation oncologists in the delineation of tumor regions during treatment planning for lung cancer, we have proposed an automated contouring algorithm based on an optimum contour selection (OCS) method for treatment planning computed tomography (CT) images with positron emission tomography (PET)/CT images. The basic concept of the OCS is to select a global optimum object contour based on multiple active delineations with a level set method around tumors. First, the PET images were registered to the planning CT images by using affine transformation matrices. The initial gross tumor volume (GTV) of each lung tumor was identified by thresholding the PET image at a certain standardized uptake value, and then each initial GTV location was corrected in the region of interest of the planning CT image. Finally, the contours of final GTV regions were determined in the planning CT images by using the OCS. The proposed method was evaluated by testing six cases with a Dice similarity coefficient (DSC), which denoted the degree of region similarity between the GTVs contoured by radiation oncologists and the proposed method. The average three-dimensional DSC for the six cases was 0.78 by the proposed method, but only 0.34 by a conventional method based on a simple level set method. The proposed method may be helpful for treatment planners in contouring the GTV regions.

Keywords: computer-assisted delineation; lung tumor; PET/CT images; level set method; gross tumor volume (GTV)

INTRODUCTION

The primary purpose of radiation therapy is to administer the highest possible dose to tumors while minimizing the dose to normal tissues and organs at risk (OARs), such as the spinal cord, esophagus and heart. The stereotactic body radiotherapy (SBRT) technique has recently been developed to meet this goal of maximal and minimal doses to the tumor and normal tissue, respectively. In performing radiotherapy, the gross tumor volume (GTV), which is defined by the gross demonstrable extent and location of a malignant growth [1], should be accurately determined, because the prescribed dose distribution in radiation treatment planning is determined individually for each tumor region. Therefore, GTV

regions have been manually delineated by radiation oncologists using treatment planning computed tomography (CT). However, the subjective manual contouring of a tumor region is tedious and time-consuming, and its reproducibility is relatively low, which could cause inter- and intra-variability of tumor regions [2–4]. Consequently, it would be not easy for many radiation oncologists to accurately delineate the GTV regions with high reproducibility and low variability.

Computer-assisted delineation methods can assist radiation oncologists in overcoming these limitations of manual contouring [3, 5–7]. In several computer-assisted methods, both morphological and functional images (such as those from CT and 18F-fluorodeoxyglucose positron emission tomography (FDG-PET)) have been employed for improving lung tumor delineation. CT is the essential modality for radiation treatment planning, because a CT image contains anatomical information and it is employed to obtain the electronic density map that is used for dose calculation. On the other hand, PET is a functional imaging modality that delineates the active tumor region, and thus it has higher sensitivity and specificity for detecting tumor tissue than CT images. El Naqa *et al.* proposed a multivalued level set method (LSM) for GTV extraction by using active contours for radiotherapy treatment planning [5]. Day *et al.* reported a region-growing method for tumor volume segmentation on FDG-PET images for rectal and anal cancer patients. In their method, the variation in the GTV was 9%, versus 37% using a simple thresholding method [3]. Strassmann *et al.* developed an atlas-based method for semi-automatically extracting tumor regions for head and neck tumors, and this method cut planning time approximately in half [6]. Ballangan *et al.* reported a region-based active contour approach for improving the accuracy of tumor delineation by using both CT and PET images for cases in which tumors abut or involve the chest walls or mediastinum [7].

This study focuses on selection of a global optimum object contour from among multiple possible delineations around a tumor. For that purpose, we have proposed an automated contouring algorithm based on an optimum contour selection (OCS) method using a LSM for treatment planning CT images combined with PET/CT images. The OCS method retrospectively determines a global optimum objective contour from among multiple active delineations around a tumor. In addition, the PET images were employed for determination of initial GTV regions to be used in the OCS method.

MATERIALS AND METHODS

This study was performed with approval by the Institutional Review Board of the Kyushu University Hospital. We employed a computer with four cores of a 3.2-GHz central processing unit (CPU) (Intel i7-3930) and a 16-GB memory on a linux system (Ubuntsu) on a Windows 7 operating system. The overall scheme of the proposed method for automated contouring of a GTV is shown in Fig. 1. First, the PET image was registered with the planning CT image through a diagnostic CT image of the PET/CT dataset [8, 9]. Initial GTV regions were obtained by thresholding the PET image at 80% of the maximum standard uptake value (SUV_{max}) within a rectangular volume of interest (VOI), which had the same geometric position as the VOI in the planning CT image. Each initial GTV location was corrected in the VOI. Finally, the GTV region was segmented using the OCS method.

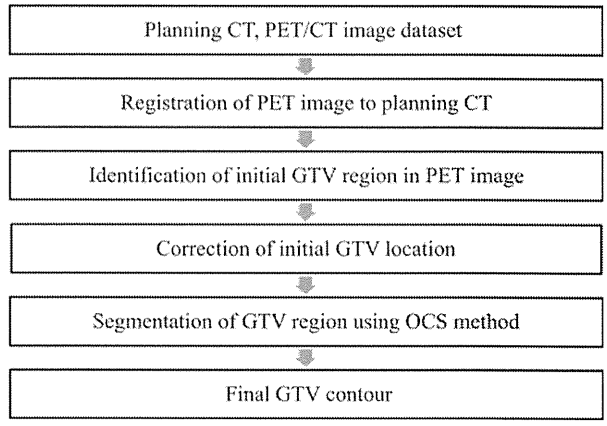

Fig. 1. An overall scheme of the proposed method for automated contouring of a GTV based on an optimum contour selection (OCS) method.

Clinical cases

Datasets consisting of planning CT and PET/CT images of six lung cancer patients (mean age: 74 years; range: 65–86 years; females: 3; males: 3; mean effective diameter of GTV: 23.8 mm; range: 17.7–29.4 mm) who had received SBRT were selected for this study. The patient characteristics are summarized in Table 1. All tumors were solid type cancers. Planning CT images of the patients were acquired with breath-holding at the end of expiration to delineate the tumor region and to calculate the dose distribution for each patient with a radiation treatment-planning (RTP) system, whereas PET/CT image sets were obtained to help the treatment planners delineate the tumor region from a functional point of view.

Planning CT images were acquired from a four-slice CT scanner (Mx 8000; Philips, Amsterdam, The Netherlands) with dimensions of 512×512 pixels, an in-plane pixel size of 0.977 mm, and a slice thickness of 2 mm. The original planning CT images were converted to isotropic images with matrix sizes of $512 \times 512 \times 234$–$313$ and an isovoxel size of 0.977 mm using a cubic interpolation method.

Table 1. Summary of patient characteristics

Patient No.	Gender	Age (years)	GTV size[a] (mm)	Tumor location	SUV^{b}_{max}	Time difference[c] (days)	Tumor CT imaging characteristics
1	female	71	17.7	RUL[d]	8.43	20	homogeneous irregular
2	female	81	25.8	RUL	4.43	2	homogeneous irregular pleural indentation
3	male	65	25.3	RUL	6.79	20	inhomogeneous irregular
4	female	67	24.2	RUL	12.2	34	homogeneous irregular vascular
5	male	75	20.2	LUL[e]	8.74	5	inhomogeneous irregular adjacent pleural
6	male	86	29.4	LUL	9.68	20	cavity irregular

[a]Effective diameter. [b]Maximum standardized uptake value. [c]Time difference between the planning CT scan and PET/CT scans. [d]Right upper lobe. [e]Left upper lobe.

PET imaging was performed on an integrated PET/CT scanner (Discovery STE; General Electric Medical Systems, Milwaukee, WI). Patients were scanned with their arms down and breathing free 60 min after the FDG injection. The PET data were acquired in the 3D mode and reconstructed with corrections for attenuation, scatter, decay, random, and dead time using a 3D ordered subsets-expectation maximization algorithm (VUE Point Plus; GE Healthcare), resulting in a 128×128 matrix with an in-plane pixel size of 5.47 mm and a slice thickness of 3.27 mm. Meanwhile, diagnostic CT images were acquired from a 16-slice CT scanner (a 512×512 matrix, an in-plane pixel size of 0.977 mm, and a slice thickness of 5 mm) in the PET/CT system.

The matrix size and isovoxel size of the PET image and diagnostic CT image in a PET/CT dataset were conformed to those ($512 \times 512 \times 234$–$313$ and 0.977 mm) of the planning CT image for registration of the PET image to the planning CT image through the diagnostic CT image. After having changed the voxel sizes, the matrix sizes of the PET and diagnostic CT images were $716 \times 716 \times 793$–$920$ and $512 \times 512 \times 234$–$313$, respectively. Because the isotropic PET images were larger than the isotropic diagnostic CT images, the PET images used for this study were cropped from the isotropic PET image by use of a template-matching technique with normalized mutual information [10], in which the diagnostic CT images were used as templates. In this template matching, image positions of the PET and diagnostic CT images were used as initial points.

The SUV was employed for identification of initial GTV regions, and it was calculated as a ratio of the radioactivity concentration of tissue at one timepoint to the injected dose of radioactivity concentration at that timepoint, divided by the body weight [11]:

$$\mathrm{SUV} = \frac{C(kBq/ml)}{D(MBq)/W(kg)}, \quad (1)$$

where C represents the radioactivity concentration in kBq/ml obtained from the pixel value in the PET image multiplied by a cross calibration factor, D is the injected dose of 18-FDG administered in MBq (decay corrected), and W is the body weight of a patient in kilograms.

The treatment-planning CT images were obtained from digital imaging and communications in medicine (DICOM) files with the personal information removed. In accordance with the definition of JCOG0403, GTV contours were determined based on a consensus between two experienced radiation oncologists with reference to the PET/CT images using an RTP system (Varian, Eclipse Ver. 6.5).

Two-step registration of PET image to planning CT image

The CT scan has the advantage of providing high-resolution images with anatomical detail, but it is not good at giving functional information about tumors. In contrast, PET images reflect the functional processes in biological bodies. To utilize both functional and anatomical information in the same coordinate system, the PET images were registered with the planning CT images.

Figure 2 illustrates a two-step registration of a PET image to a planning CT image. In the first step, a diagnostic CT image of PET/CT was registered with a planning CT image by using an affine transformation, which was calculated by manually selecting nine feature points. These points are the apexes of the left and right lungs, the most anterior points of the left and right lungs, the most posterior points of the left and right lungs, the most lateral points of the left and right lungs, and the most superior point of the diaphragm from treatment-planning CT images and diagnostic CT images of PET/CT image sets. Twelve elements in the affine transformation matrix were calculated using a least squares method based on a singular value decomposition. In the second step, the PET images were registered to the treatment-planning CT images by using the same transformation matrix, because the PET image was scanned using the same coordinate system as used for the diagnostic CT image of PET/CT. However, the two-step registration was performed in terms of the left and right lungs, rather than with reference to a lung tumor.

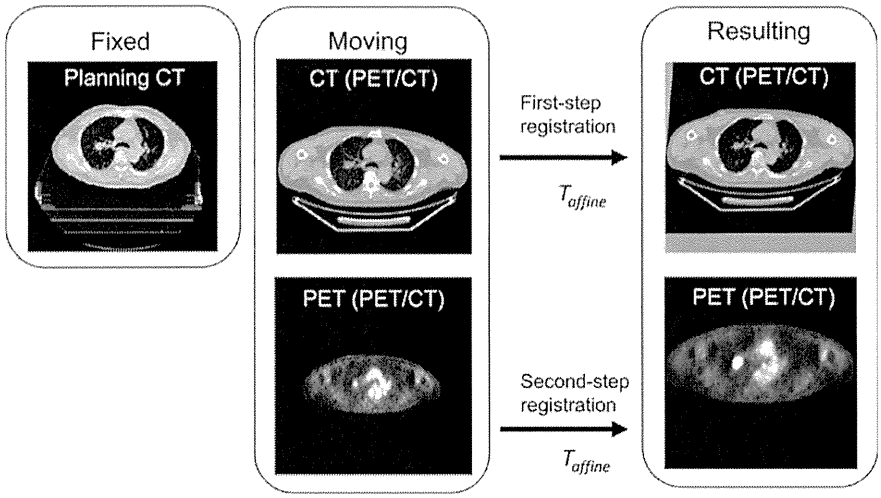

Fig. 2. An illustration of a two-step registration of a PET/CT image set to a planning CT image.

Therefore, an initial lung tumor identified on the PET image should be locally aligned with the planning CT image, as described in a later section.

Identification of initial GTV regions

Initial GTV regions were determined by thresholding the PET images by a certain percentage of the SUV_{max}, because brighter tumor regions in PET images indicate regions where tumor cells may be active.

First of all, a rectangular VOI, which was slightly larger than a circumscribed parallelepiped of a tumor, was determined in the planning CT image by manually selecting the minimum and maximum coordinates of the circumscribed parallelepiped, and calculating its widths in the x, y and z directions. The PET image was thresholded at a certain percentage of the SUV_{max} within the VOI to identify the initial GTV region. We can assume that the region of interest (ROI) size and location would not affect the segmentation results, because the initial GTV regions were determined based on the tumor SUV, which was independent of the ROI.

In a preliminary study, the suitable threshold percentages of the SUV_{max} for segmentation of initial tumor regions on the PET images were determined for all cases by changing the percentage of SUV_{max} from 30 to 80% as a threshold value in the VOI. Figure 3 shows an example that compares the tumor regions (white regions) segmented by different threshold values and the GTV contours (red lines) determined by radiation oncologists for Case 6. The comparison for all cases revealed that regions segmented at 80% of the SUV_{max} were suitable as the initial GTV regions for the proposed method, because the initial regions should be inside the desired contours in the proposed method. Figure 4 illustrates the initial regions (red regions) in a VOI. All initial regions were located inside the tumor region in this case, and they should be as large as possible to prevent potential cavities due to inhomogeneous inner regions of lung tumors, and to reduce the calculation time.

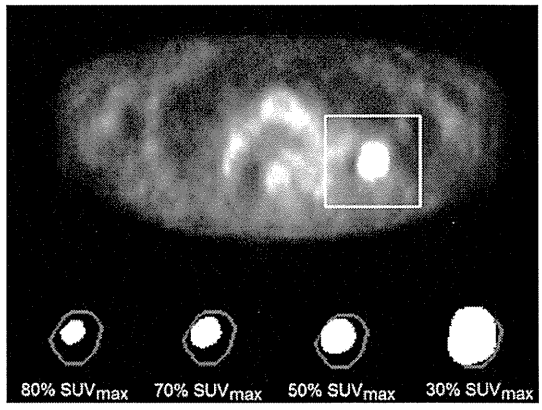

Fig. 3. A comparison between the tumor regions (white regions) segmented by different threshold values and a GTV contour (red line) determined by radiation oncologists for Case 6.

Correction of initial GTV location in a ROI of a planning CT image

To register PET/CT images and planning CT images, Cai *et al.* performed a validation study of CT and PET lung image registration based on a chamfer-matching method, with registration errors of 2–3 mm in the transverse plane, 3–4 mm in the longitudinal direction, and about 1.5 degrees in rotation [12]. Mattes *et al.* proposed a free-form deformation method, with overall errors ranging from 0 to 6 mm [13]. Figure 5 illustrates the discrepancies in location and shape of tumor regions between the CT and PET images after the two-step registration mentioned above. These discrepancies might be caused by respiratory motion, inhomogeneous

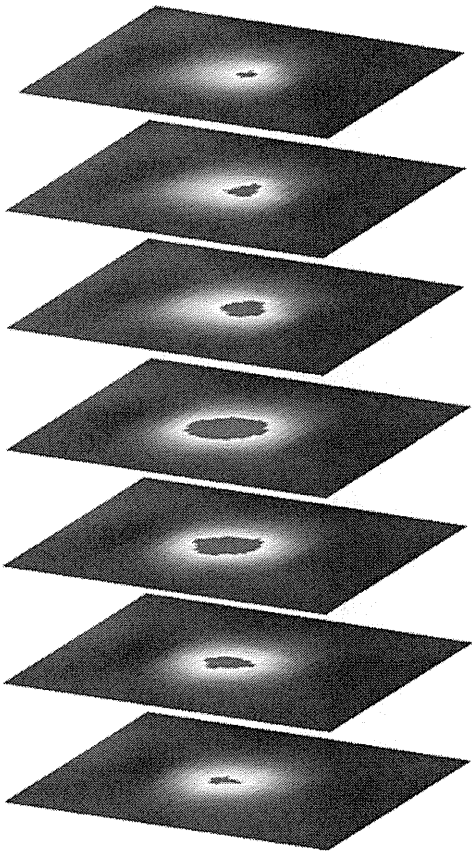

Fig. 4. An illustration of initial regions (red regions) in a VOI.

radioactivity concentrations in the GTV regions, or the large time intervals between the PET/CT and planning CT scans.

To correct the tumor location described above, the centroid of an initial GTV region obtained from a PET image was aligned with the center of the ROI in a planning CT image on a slice-by-slice basis. The ROI was the same as the transverse plane of the VOI used for the identification of the initial GTV regions. In this process, only the ROI region (not the entire PET image) was moved to adjust the tumor location. Figure 6 illustrates the correction of an initial GTV location in an ROI of a planning CT image by alignment of the initial region obtained from a PET image with the center of the ROI in each slice. The location discrepancy between the initial GTV region and the lung tumor was successfully corrected after the alignment.

Segmentation of GTV regions using an OCS method

The final GTVs were segmented by applying the OCS method to the initial region as determined on the PET images. The basic concept of the OCS method is to retrospectively select a global optimum object contour from among multiple active delineations with an LSM around tumors. In the OCS method, the LSM [14] is employed for searching for the optimum object contour in the relationship between the average speed function value on an evolving curve and the evolution time.

In the first step, the GTV contour and the speed function value obtained by the LSM were recorded at each evolution time from the initial GTV region until the evolution time reached 10 000 or the evolving curve reached the edge of the ROI in the planning CT image. The level set function $\varphi(x,y,t)$ was updated from the initial GTV region contour by using the following discrete partial differential equation:

$$\varphi^{n+1}(x,y,t) = \varphi^{n}(x,y,t) - \Delta t F(x,y,t)|\nabla\varphi^{n}(x,y,t)|, \quad (2)$$

where n is the evolution number, t is the evolution time, Δt is the evolution time interval, and $F(x,y,t)$ is the speed function. The evolution time is the time of the contour deformation in updating the discrete partial differential equation. The zero level set of $\varphi(x,y,t)$, which corresponds to the contour of the segmented region, moves according to the speed function $F(x,y,t)$ in the 3D level set function. The zero level set function, i.e. the evolving curve, moves according to the following speed function $F(x,y,t)$:

$$F(x,y,t) = b(x,y)\{1 - \nu\kappa(x,y,t)\}, \quad (3)$$

$$b(x,y) = \frac{1}{1 + |\nabla\{G(x,y) \otimes I(x,y)\}|}, \quad (4)$$

where $b(x,y)$ is the function of the edge indicator, $G(x,y)$ is the Gaussian function, $I(x,y)$ is the planning CT image to be processed, $\otimes$ denotes convolution, ν is a constant, and $\kappa(x,y,t)$ is the curvature. The edge indicator function $b(x,y)$ and speed $F(x,y,t)$ would be small around the edge, whereas the functions $b(x,y)$ and $F(x,y,t)$ would be large in relatively homogeneous regions.

In the second step, the GTV contour was determined from the optimum contour derived using the LSM by searching for the minimum point in the relationship between the evolution time and the average speed function value on an evolving curve, based on the steepest descent method (SDM). To avoid local minimum traps, the average speed function was smoothed by a median filter, and the smoothed function was resampled by a larger interval than the original one, before applying the SDM.

Evaluation of the proposed method

The performance of the proposed method was evaluated using a Dice similarity coefficient (DSC) [15]. The DSC denotes the degree of region similarity between the GTV gold standard region and the GTV region obtained by the proposed method. The DSC was calculated by the following equation:

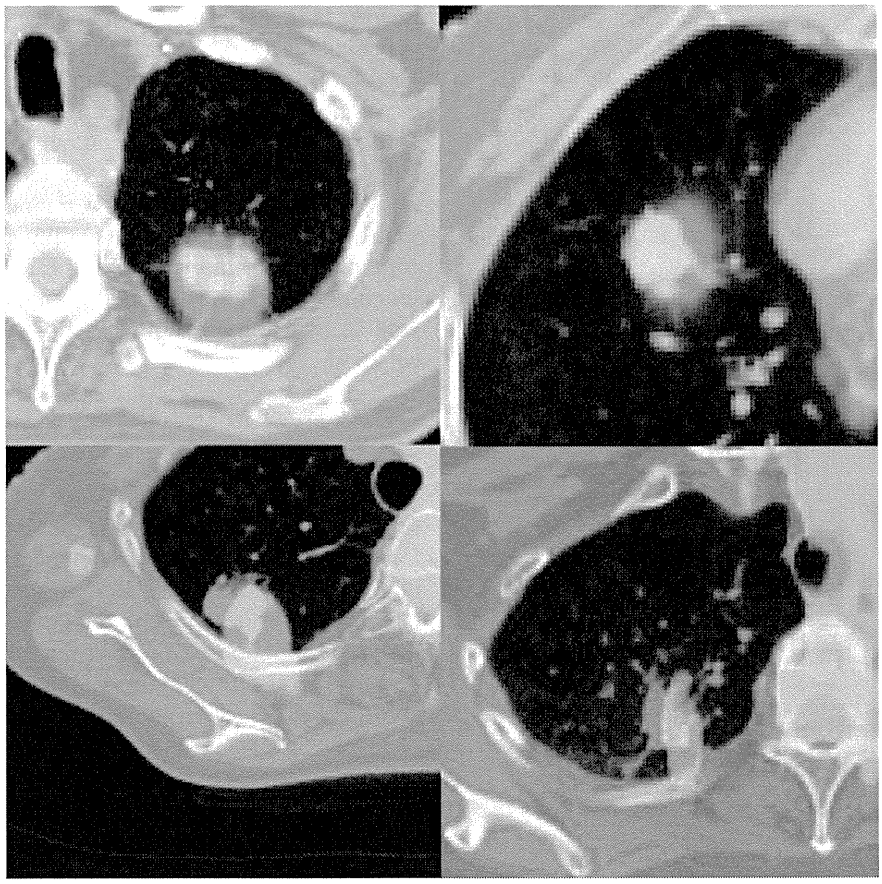

Fig. 5. Illustrations of discrepancies in location and shape of tumor regions between the CT and PET images after the two-step registration.

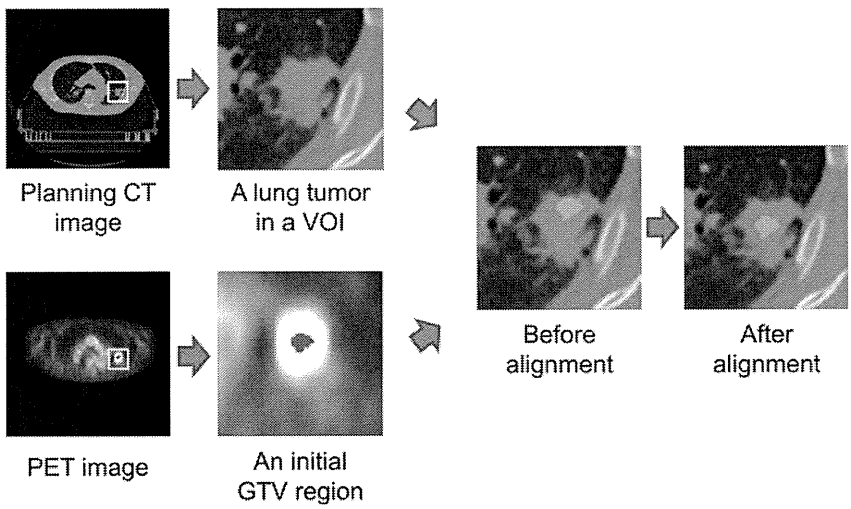

Fig. 6. An illustration of the correction of an initial GTV location in a ROI of a planning CT image by alignment of the initial region obtained from a PET image with the center of the ROI on a slice-by-slice basis.

$$DSC = \frac{2n(T \cap D)}{n(T) + n(D)}, \quad (5)$$

where T is the GTV gold standard region determined by two radiation oncologists, D is the GTV region contoured by the proposed method, $n(T)$ is the number of pixels in the region T, $n(D)$ is the number of pixels in the region D, and $n(T \cap D)$ is the number of logical AND pixels between T and D. The DSC ranges from 0 (no overlap between T and D) to 1 (T and D are identical). A DSC value of greater than 0.7, which denotes a good agreement between T and D, has been generally accepted in the medical field [16–18].

The GTV regions were obtained from the DICOM for radiation therapy (DICOM-RT) files. The isotropic GTV region was used as the gold standard, which was produced by use of a shape-based interpolation [19] for matching with the isotropic planning CT image with an isovoxel size of 0.977 mm.

The DSC for each case was calculated in two different ways. First, the average value of the DSCs was calculated based on a 2D slice, yielding the 2D average DSC. Second, the DSC was calculated from a 3D planning CT image to obtain the 3D DSC.

To evaluate the usefulness of the proposed method, a conventional method was compared with the proposed method. In the identification of an initial GTV region step, the center-point of each ROI was used as the initial region without using PET images. In the segmentation of GTV regions using an OCS method step, a fast LSM [20] was used instead of the OCS method. In the fast LSM, the threshold for the value of average speed function was manually optimized based on all six cases, and was 0.015 for this study. In contrast, the proposed method adaptively determines the threshold value depending on the GTV regions, which is one of the advantages of the proposed method. Those two methods were fully automatic except for determination of the VOI around the GTV regions.

RESULTS

Figure 7a illustrates the GTV contours, which were delineated a number of times by the proposed method on the planning CT image for Case 6 at evolution times of 500, 2000, 4000 and 6000. Figure 7b shows the relationship in the LSM between the evolution time and the average speed function value on an evolving curve. In Case 6, the average speed function $\overline{F(t)}$ as a function of evolution time t converges to the global minimum between evolution times of 2000 and 4000. At an evolution time of 500, the segmented GTV region is relatively small and corresponds to a larger $\overline{F(t)}$ as a result of the low contrast inside the segmented region. For evolution times of 2000 and 4000, the GTV contours seem to be well extracted and approach the minimum value of $\overline{F(t)}$ due to the tumor edge. At an evolution time of 6000, the estimated GTV contour was too large, and it had a greater $\overline{F(t)}$ value due to the low contrast outside the tumor region. Therefore, the optimum contour can be determined by detecting the minimum point in the relationship between the average speed function and the evolution time.

The resultant GTVs were visually investigated and categorized in terms of the tumor CT imaging characteristics [21], which were determined by a radiologist (HY) with more than 5 years of experience. Figure 8 compares the segmentation results of the proposed method and the conventional method for six types of lung tumors classified according to tumor CT imaging characteristics. For Case 1, the proposed method provided a GTV contour that is closer to the GTV gold standard on the irregular tumor margin. The evolving curve stopped at almost the same position as the GTV gold standard when the

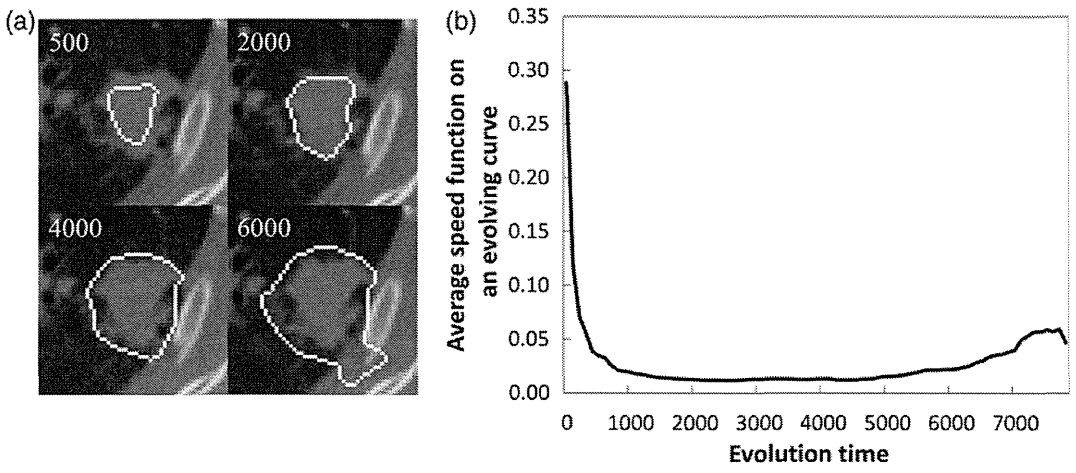

Fig. 7. Illustrations of (**a**) contours on a planning CT image at evolution times of 500, 2000, 4000 and 6000, and (**b**) the relationship in the LSM between the evolution time and the average speed function on a moving front line.

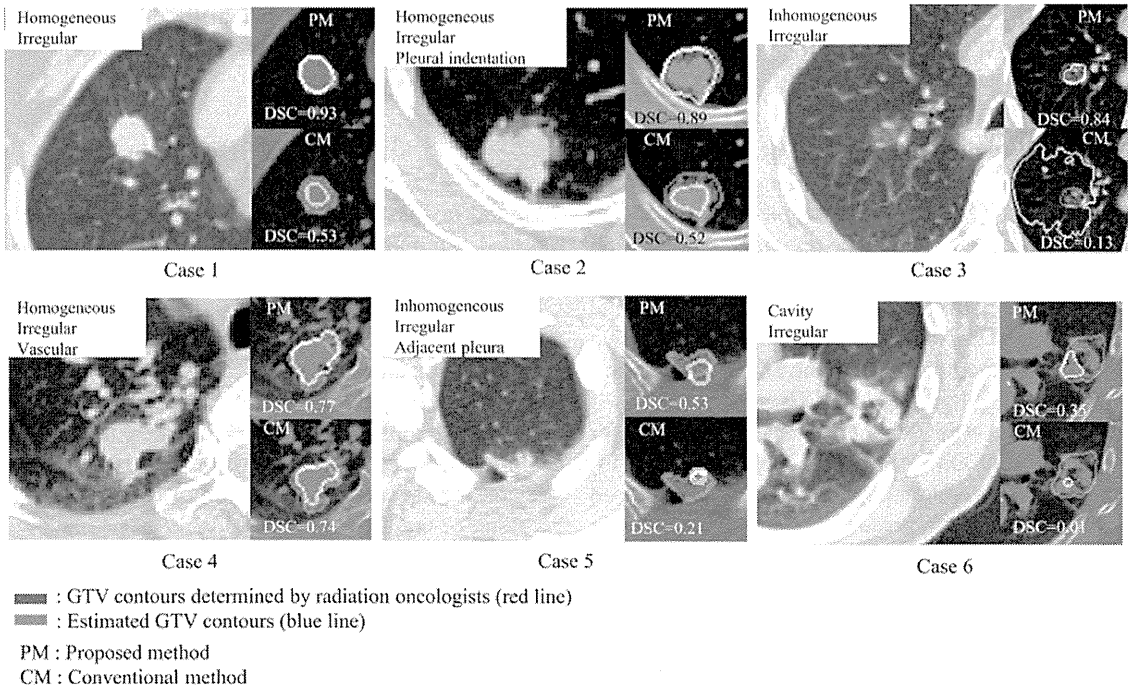

Fig. 8. A comparison between results of the proposed method and conventional method in terms of tumor CT imaging characteristics.

Table 2. DSCs between GTV gold standard regions and GTV regions segmented by the proposed method and the conventional method for six cases

Method	DSC	Case number						Mean
		1	2	3	4	5	6	
Conventional method	2D[a]	0.30	0.38	0.54	0.49	0.46	0.44	0.44
	3D[b]	0.40	0.12	0.52	0.08	0.40	0.52	0.34
Proposed method	2D	0.74	0.63	0.80	0.83	0.78	0.65	0.74
	3D	0.81	0.71	0.80	0.83	0.81	0.71	0.78

[a]Mean for 2D DSCs in all slices with GTV contours between the two methods. [b]3D DSC for whole GTV volumes between the two methods.

proposed method was used, but it was terminated before reaching the GTV gold standard when the conventional method was used, due to a fixed threshold value for the speed function. For Case 2, the proposed method better segmented a homogeneous and irregular tumor with pleural indentation with a higher DSC of 0.89. For the inhomogeneous and irregular tumor region in Case 3, the proposed method showed a higher DSC of 0.84 with the GTV gold standard, whereas the conventional method overestimated the GTV because of the unclear edge of the tumor. For Case 4, the results of both the proposed method and conventional method were comparable for homogeneous and irregular tumors adjacent to vascular tissues. For Case 5 in Fig. 8, neither method was able to correctly extract reasonable GTVs, because the tumor contacted a chest wall, and there appeared to be no boundary between the tumor and the chest wall. To extract this type of GTV, we will need to develop a method for estimating the chest wall boundary in the future. For Case 6, the proposed method extracted only a part of the GTV region with cavities, whereas the evolving curve in the conventional method was terminated inside a very small region of the GTV. Consequently, we need a method for more accurately segmenting initial regions, so that they cover the cavity regions to avoid the effect of low speed values inside tumors.

Table 2 shows the DSCs between the GTV gold standard region and the GTV segmented by the proposed method and the conventional method for six cases. The average 3D DSC between the GTV gold standards contoured by radiation oncologists and the GTV regions obtained by the proposed

method was 0.78 for six cases. This result was higher than the average DSC of 0.34 obtained by the conventional method.

DISCUSSION

To evaluate the usefulness of initial regions obtained from PET images, a method without using PET images was compared with the proposed method. In this method, the center-point of each ROI was used instead of using the initial regions obtained from PET images, but the other steps of the method were exactly the same as the proposed method. This method differed from the conventional method, which was used for comparison in Table 2. As a result, the mean 3D DSC of this method was 0.56, which was much lower than the 0.78 obtained by the proposed method. Therefore, we believe that the initial regions on the PET images could be useful for segmentation of lung tumors in the proposed method.

In this paragraph, three studies [5, 22, 23] on automatic delineation methods for lung cancer radiation therapy were compared with the proposed method, because they were evaluated using the DSC. El Naqa *et al.* [5] developed a segmentation method based on CT, PET and magnetic resonance (MR) images by applying a multivalued LSM. The average DSC was 0.90 for a phantom study, not patient studies. In general, MR imaging is not applied for lung cancer patients. Wanet *et al.* [22] validated a gradient-based segmentation method for performing GTV delineation on FDG-PET of non-small-cell lung cancer patients using surgical specimens in comparison with threshold-based approaches and CT. The average DSC was 0.58 to 0.62 on CT images and 0.62 to 0.68 on PET images. Markel *et al.* [23] developed an approach based on a combined decision tree with *k*-nearest neighbors to classify voxels based on their first-, second-, and higher-order statistics as well as structural and Tamura features. The approach was able to segment tumors with an average DSC of 0.607 for 31 lung cancer patients. On the other hand, the average DSC obtained by the proposed method was 0.78 for six patients, which was lower than for the phantom study, but higher than for the patient study.

The mean calculation time of the proposed method was 16 min 27 s for the six cases using the general personal computer. This was less than the mean spending time of the conventional method, which was 27 min 54 s, because the proposed method could terminate the evolution of moving contours when the tumor edges were blurred, but the conventional method could not, as is shown for Case 3 in Fig. 8. Therefore, the proposed method was more efficient than the conventional method. However, the computation time can be reduced with the use of a general-purpose graphical processing unit (GP-GPU) for clinical practice.

Six cases with various types of tumor CT imaging characteristics were selected for this study, but the proposed method should be applied to many types of tumors in the future so as to improve the segmentation accuracy, especially for cavity-type tumors and tumors abutting the chest wall. In addition, independent databases obtained from different institutions and planning CT scanners should be used in order to improve the robustness of the proposed method.

CONCLUSION

We proposed an automated contouring method based on the OCS method for treatment-planning CT images with PET/CT images. In the proposed method, initial GTV regions were determined from 80% of SUV_{max} on the PET images, and then global optimum GTV contours from among multiple possible delineations around lung tumors were selected. The proposed method was more accurate and efficient than the conventional method, and thus may be useful for assisting radiation oncologists in contouring lung GTV regions.

FUNDING

Funding to support this study and the payment of the Open Access publication charges for this article was provided by the Okawa Foundation for Information and Telecommunications, the Ministry of Education, Culture, Sports, Science, and Technology (MEXT), and by Grants-in-Aid for Scientific Research on Innovative Areas (24103707) and Scientific Research (c) (22611011), 2012.

REFERENCES

1. International Commission on Radiation Units and Measurements. Prescribing, Recording, and Reporting Photon Beam Therapy. *Supplement to ICRU Report 50*. Bethesda, MD: ICRU, 1999, 833–4.
2. Van de Steene J, Linthout N, de Mey J *et al.* Definition of gross tumor volume in lung cancer: inter-observer variability. *Radiol Oncol* 2002;**62**:37–49.
3. Day E, Betler J, Parda D *et al.* Region growing method for tumor volume segmentation on PET images for rectal and anal cancer patients. *Med Phys* 2009;**36**:4349–58.
4. Nakamura K, Shioyama Y, Tokumaru S *et al.* Variation of clinical target volume definition among Japanese radiation oncologists in external beam radiotherapy for prostate cancer. *Jpn J Clin Oncol* 2008;**38**:275–80.
5. El Naqa I, Yang D, Apte A *et al.* Concurrent multimodality image segmentation by active contours for radiotherapy treatment planning. *Med Phys* 2007;**34**:4738–49.
6. Strassmann G, Abdellaoui S, Richter D *et al.* Atlas-based semi-automatic target volume definition (CTV) for head-and-neck tumors. *Int J Radiat Oncol Biol Phys* 2010;**78**:1270–6.
7. Ballangan C, Wang XY, Feng DG. Lung tumor delineation in PET-CT images based on a new segmentation energy. *IEEE Nucl Sci Symp Med Imaging Conf (NSS/MIC)* 2011;3202–5.
8. Hill DL, Batchelor PG, Holden M *et al.* Medical image registration. *Phys Med Biol* 2001;**46**:R1–45.

9. Burger W, Burge M. *Digital Image Processing: an Algorithmic Introduction Using Java*, 1st edn. New York: Springer, 2008.
10. Pluim JPW, Maintz JBA, Viergever MA. Mutual-information-based registration of medical images: a survey. *IEEE Trans Med Imaging* 2003;**22**:986–1004.
11. Boellaard R. Standards for PET image acquisition and quantitative data analysis. *J Nucl Med* 2009;**50**(Suppl 1): 11S–20S.
12. Cai J, Chu JC, Recine D *et al.* CT and PET lung image registration and fusion in radiotherapy treatment planning using the chamfer-matching method. *Int J Radiat Oncol Biol Phys* 1999;**43**:883–91.
13. Mattes D, Haynor DR, Vesselle H *et al.* PET-CT image registration in the chest using free-form deformation. *IEEE Trans Med Imaging* 2003;**22**:120–8.
14. Sethian JA. Level Set Methods and Fast Marching Methods: Evolving Interfaces in Computational Geometry, Fluid Mechanics, Computer Vision, and Materials Science. Cambridge: Cambridge University Press, 1999.
15. Crum WR, Camara O, Hill DL. Generalized overlap measures for evaluation and validation in medical image analysis. *IEEE Trans Med Imaging* 2006;**25**:1451–61.
16. Zijdenbos AP, Forghani R, Evans AC. Automatic "pipeline" analysis of 3-D MRI data for clinical trials: application to multiple sclerosis. *IEEE Trans Med Imaging* 2002;**21**: 1280–91.
17. Keall PJ, Mageras GS, Balter JM *et al.* The management of respiratory motion in radiation oncology report of AAPM Task Group 76. *Med Phys* 2006;**33**:3874–900.
18. Gaede S, Olsthoorn J, Louie AV *et al.* An evaluation of an automated 4D-CT contour propagation tool to define an internal gross tumour volume for lung cancer radiotherapy. *Radiother Oncol* 2011;**101**:322–8.
19. Herman GT, Zheng J, Bucholtz C. Shape-based interpolation. *IEEE Comput Graph Appl* 1992;**12**:69–79.
20. Iwashita Y, Kurazume R, Tsuji T *et al.* Fast implementation of level set method and its real-time applications. *Conf Proc IEEE Int Conf Syst Man Cybern* 2004;**7**:6302–7.
21. Kawakami Y, Ogura S. The outline of the general rule for clinical and pathological record of lung cancer. *Nihon Rinsho* 2000;**58**:999–1004.
22. Wanet M, Lee JA, Weynand B *et al.* Gradient-based delineation of the primary GTV on FDG-PET in non-small cell lung cancer: a comparison with threshold-based approaches, CT and surgical specimens. *Radiother Oncol* 2011;**98**:117–25.
23. Markel D, Caldwell C, Alasti H *et al.* (26 February 2013) Automatic segmentation of lung carcinoma using 3D texture features in 18-FDG PET/CT. *Int J Mol Imaging* 2013; **2013**:980769, 10.1155/2013/980769.

Journal of Radiation Research, 2014, 55, 146–153
doi: 10.1093/jrr/rrt098 Advance Access Publication 16 August 2013

Boron neutron capture therapy outcomes for advanced or recurrent head and neck cancer

Minoru SUZUKI[1,*], Ituro KATO[4], Teruhito AIHARA[5], Junichi HIRATSUKA[6], Kenichi YOSHIMURA[7], Miyuki NIIMI[7], Yoshihiro KIMURA[8], Yasunori ARIYOSHI, Shin-ichi HAGINOMORI[9], Yoshinori SAKURAI[2], Yuko KINASHI[3], Shin-ichiro MASUNAGA[1], Masanori FUKUSHIMA[7], Koji ONO[1] and Akira MARUHASHI[1]

[1]Particle Radiation Oncology Research Center, Research Reactor Institute, Kyoto University, 2-1010, Asashiro-nishi, Kumatori-cho, Sennan-gun, Osaka 590-0494, Japan
[2]Department of Radiation Life Science, Research Reactor Institute, Kyoto University, 2-1010, Asashiro-nishi, Kumatori-cho, Sennan-gun, Osaka 590-0494, Japan
[3]Division of Radiation Safety, Research Reactor Institute, Kyoto University, 2-1010, Asashiro-nishi, Kumatori-cho, Sennan-gun, Osaka 590-0494, Japan
[4]Department of Oral and Maxillofacial Surgery II, Graduate School of Dentistry, Osaka University, 1-8, Yamada-Oka, Suita, Osaka 565-0871, Japan
[5]Department of Otolaryngology and Head and Neck Surgery, Kawasaki Medical School, 577, Matsushima, Kurashiki-City, Okayama 701-0192, Japan
[6]Department of Radiation Oncology, Kawasaki Medical School, 577 Matsushima, Kurashiki-City, Okayama 701-0192, Japan
[7]Department of Clinical Trial Design and Management, Translational Research Center, Kyoto University Hospital, 54 Kawaracho, Shogoin, Sakyo-ku, Kyoto 606-6507, Japan
[8]Department of Dentistry and Oral Surgery, Osaka Medical College, 2-7, Daigaku-machi, Takatsuki Ciy, Osaka 569-8686, Japan
[9]Department of Otolaryngology, Osaka Medical College, 2-7, Daigaku-machi, Takatsuki City, Osaka 569-8686, Japan
*Corresponding author: Particle Radiation Oncology Research Center, Research Reactor Institute, Kyoto University, 2-1010, Asashiro-nishi, Kumatori-cho, Sennan-gun, Osaka 590-0494, Japan. Tel: +81-724-51-2390; Fax: +81-724-51-2627; Email: msuzuki@rri.kyoto-u.ac.jp

(Received 28 February 2013; revised 16 July 2013; accepted 17 July 2013)

We retrospectively review outcomes of applying boron neutron capture therapy (BNCT) to unresectable advanced or recurrent head and neck cancers. Patients who were treated with BNCT for either local recurrent or newly diagnosed unresectable head or neck cancers between December 2001 and September 2007 were included. Clinicopathological characteristics and clinical outcomes were retrieved from hospital records. Either a combination of borocaptate sodium and boronophenylalanine (BPA) or BPA alone were used as boron compounds. In all the treatment cases, the dose constraint was set to deliver a dose <10–12 Gy-eq to the skin or oral mucosa. There was a patient cohort of 62, with a median follow-up of 18.7 months (range, 0.7–40.8). A total of 87 BNCT procedures were performed. The overall response rate was 58% within 6 months after BNCT. The median survival time was 10.1 months from the time of BNCT. The 1- and 2-year overall survival (OS) rates were 43.1% and 24.2%, respectively. The major acute Grade 3 or 4 toxicities were hyperamylasemia (38.6%), fatigue (6.5%), mucositis/stomatitis (9.7%) and pain (9.7%), all of which were manageable. Three patients died of treatment-related toxicity. Three patients experienced carotid artery hemorrhage, two of whom had coexistent infection of the carotid artery. This study confirmed the feasibility of our dose-estimation method and that controlled trials are warranted.

Keywords: boron neutron capture therapy; head and neck tumors

INTRODUCTION

The incidence rate in Japan of head and neck cancer during 2008 was 16.3/100 000 population, and approximately 7800 cases died during 2011. Both the incidence and mortality rates of head and neck cancer are increasing. Aggressive and combined local treatment including surgery and chemoradiation has been applied to advanced head and neck cancer, because the prognosis for patients with recurrent disease is generally poor. Unfortunately, the rate of local recurrence has been reported at 20–57% following aggressive local treatment.

For unresectable recurrent head and neck cancer, chemotherapy alone has been considered standard treatment. However, the therapeutic effect of chemotherapy is limited to palliative settings. Reirradiation with or without chemotherapy has been investigated since the 1990s as curative treatment for unresectable advanced or recurrent head and neck cancer. Single or multicenter studies of combined treatment with reirradiation and chemotherapy have demonstrated a small number of patients with long-term survival [1, 2]. Although substantial morbidity related to reirradiation has been reported in these studies, reirradiation with or without chemotherapy has the potential to cure unresectable recurrent head and neck cancer.

The rationale for application of reirradiation with boron neutron capture therapy (BNCT) for recurrent head and neck cancer is based on the unique property of BNCT, which can deposit a large dose gradient between the tumor and surrounding normal tissues. BNCT is based on the following nuclear reaction. Nonradioactive isotope ^{10}B atoms that absorb low-energy (<0.5 eV) neutrons (thermal neutrons) disintegrate into an alpha (^{4}He) particle and a recoiled lithium nucleus (^{7}Li). These particles deposit high energy along their very short path (<10 μm) [3]. Thus, only malignant cells with ^{10}B are destroyed following thermal neutron irradiation. Theoretically, any normal cells abutting the cancer cells are spared from high linear energy transfer (LET) irradiation by ^{4}He and ^{7}Li particles.

In 2001, a patient with recurrent parotid gland tumor after standard therapies including surgery, radiotherapy and chemotherapy was referred to the Kyoto University Research Reactor Institute (KURRI) from Osaka University, Graduate School of Dentistry. The patient was treated with BNCT at KURRI, which was the first such attempt worldwide [4]. In the first case, locoregional control of the patient was achieved for 7 years until the patient died of intercurrent disease. This promising initial result prompted clinical trials of BNCT for head and neck cancer in Japan and Finland, and several case reports of BNCT for recurrent head and neck tumors have been published by our research group [5, 6].

To investigate the efficacy and safety of applying BNCT to head and neck cancers, we conducted an outcomes study using the records of consecutive patients who were treated with BNCT.

MATERIALS AND METHODS

Patients

Patients who were treated with BNCT at KURRI for either locoregionally recurrent or newly diagnosed head or neck cancers between December 2001 and September 2007 were identified in the hospital's medical records. Clinicopathological characteristics and clinical outcomes of the patients were retrieved from these records. This study was performed according to Ethical Guidelines for Epidemiological Research by the Japanese Government. Informed consent was obtained according to the guidelines. The study protocol was approved by the Ethical Review Board of each medical institute.

Overview of BNCT for head and neck tumors

Boronophenylalanine (BPA) and borocaptate sodium (BSH), which have been employed in clinical BNCT trials for malignant glioma or melanoma, were used in the present study of BNCT for head and neck cancers. All the patients showed good accumulation of BPA in the tumor in an ^{18}F-BPA-positron emission tomography (PET) study before BNCT. In 72 cases, BPA in fructose solution (BPA-f) was intravenously administered at a dose of 250 or 500 mg/kg. A further 15 cases received both BSH (5 g/body) dissolved in 50% physiological saline solution and BPA-f (250 mg/kg) intravenously. Two different treatment schedules were adopted in the cases treated with BPA alone. Until May 2004, BPA was administered at a dose of 250 or 500 mg/kg in 1–2 h, followed by epithermal neutron irradiation within 15 min after finishing administration of the BPA-f solution. From June 2004, BPA was administered at a dose of 500 mg/kg in 3 h at a rate of 200 mg/kg/h for the initial 2 h, and at the reduced speed of 100 mg/kg/h for the remaining 1 h. Epithermal neutron irradiation was carried out during the final 1 h during infusion of BPA at a speed of 100 mg/kg/h. In cases administered both BSH and BPA, the epithermal neutron irradiation was started 12 h and 1 h after finishing of administration of BSH and BPA, respectively. The irradiation time was determined so that the maximum dose to the surrounding normal tissues (oral mucosa in the majority of the cases and skin in the remainder) would be <10–12 Gy-eq.

Radiation treatment planning

Details of the procedures for radiation treatment planning with a Simulation Environment for Radiotherapy Applications (SERA) system and the Japan Atomic Energy Research Institute's Computational Dosimetry System, which are currently available BNCT treatment-planning systems, have been published [7].

SERA has been described in our previous report on a treatment-planning study of BNCT for multiple liver tumors [8]. We describe the procedure briefly here. First, the computed tomography (CT) images of each patient with head

and neck tumors were inputted to the SERA system. On each slice of the CT image, the volume for the gross tumor volume and surrounding normal tissues including muscle, adipose tissue, skin and mucosa, bone and air (e.g. oral cavity and airway) were delineated. The behavior of thermal neutrons in the body is heavily affected by the proton density in the tissues; therefore, bone and air should be depicted separately.

Biological effects of boron compounds depend on their microdistribution in the tissues and the morphological characteristics of the target cells. Therefore, compound biological effectiveness (CBE) factors were used as alternative relative biological effectiveness (RBE) factors [3]. BNCT consists of mixed radiation fields, with three different types of radiation as follows: (i) low-LET γ rays, resulting primarily from the capture of thermal neutrons by normal tissue hydrogen atoms [$^{1}H(n,\gamma)^{2}H$] and contaminating γ-rays from the neutron beam port (bismuth-surface), the collimator and the irradiation room wall; (ii) high-LET protons, produced by the scattering of fast neutrons [$^{1}H(n,n)^{1}H$] and from the capture of thermal neutrons by nitrogen atoms [$^{14}N(n,p)^{14}C$]; and (iii) high-LET, heavier-charged particles consisting of ^{4}He nuclei and ^{7}Li ions, released as products of thermal neutron capture reactions (BNCR) with ^{10}B [$^{10}B(n,\alpha)^{7}Li$]. The doses by epithermal neutron beam in the absence of ^{10}B comprise the low-LET γ-ray dose plus the high-LET proton dose as described above. The CBE factor was calculated using the following equation.

$$\text{CBE factor} = (D_{X-ray} - D_{beam} \times RBE_{beam})/D_{BNCR},$$

where $D_{X\text{-}ray}$, D_{beam} and D_{BNCR} are the doses of the reference X-ray, the epithermal neutron beam, and the ^{4}He nuclei and ^{7}Li particles derived from the $^{10}B(n,\alpha)^{7}Li$ reaction required for equal biological effect; RBE_{beam} is the RBE for the epithermal neutron beam alone in the absence of ^{10}B. The RBE or CBE factors for the tumor and normal tissues are summarized in Table 1.

The parameters and values required in the calculation with SERA include the ^{10}B concentrations in the tumor or normal tissues, the thermal neutron fluence, the nitrogen composition of the tissues, the RBE of each component of the beam, and the CBE factors of the boron compound. The accumulation of BPA in the tumor and normal tissue was imaged and quantified as a tumor/blood ratio (T/B ratio) by an ^{18}F-BPA positron emission tomography (PET) study before BNCT, as previously described [4]. In the ^{18}F-BPA PET study performed before BNCT, ^{18}F-BPA was injected through the same route as for BNCT on the day of treatment. ^{10}B concentrations in the tumor during irradiation were estimated by multiplying the T/B ratio by ^{10}B concentrations in the normal tissue during irradiation. In the present study, ^{10}B concentrations in the normal tissue were assumed to be equal to blood ^{10}B concentrations during irradiation. ^{10}B concentrations in the blood during irradiation were calculated as the mean ^{10}B concentrations in the blood sampled just before and just after the irradiation, because ^{10}B concentrations in blood should have been decreased after the finish of injection of BPA.

Thermal neutron fluence was measured by radioactivation of gold wires (0.25 mm in diameter and 1.0 cm long) placed on the skin surface of the lesion. The SERA system was run for the dose calculation after all the parameters were entered. The dose–volume histogram (DVH) parameters, as well as the maximum, mean and minimum doses given to the gross tumor volume, were evaluated for each case.

Evaluation of efficacy and safety

Tumor response evaluations were performed with either CT or magnetic resonance imaging (MRI) performed within 6 months after BNCT using the RECIST (Response Evaluation Criteria in Solid Tumors) criteria version 1.0. Overall survival (OS) time was calculated from the initiation of BNCT to the date of any cause of death or last confirmed day of survival, whichever occurred first. Progression-free survival (PFS) time was calculated from the initiation of BNCT to the progression or death from any cause, whichever occurred first. Adverse events were graded according to the Common Terminology Criteria for Adverse Events v3.0 (CTCAE v3.0). Following BNCT, 40% of patients received other therapies; therefore, adverse effects that occurred within 1 month after BNCT were analyzed.

Table 1. RBE and CBE factors used for conversion of physical dose (Gy) to photon-equivalent dose (Gy-eq)

BNCT dose components	Tumor	Skin	Oral mucosa
^{10}B (n, α) ^{7}Li	3.8 ($CBE_{for\ BPA}$)	2.5 ($CBE_{for\ BPA}$)	4.9 ($CBE_{for\ BPA}$)
	2.5 ($CBE_{for\ BSH}$)	0.8 ($CBE_{for\ BSH}$)	0.3 ($CBE_{for\ BSH}$)
^{14}N (n, p) ^{14}C	3.0	3.0	3.0
Fast neutron	3.0	3.0	3.0
gamma-ray	1.0	1.0	1.0

BNCT = boron neutron capture therapy, RBE = relative biological effectiveness, CBE = compound biological effectiveness, BPA = boronophenylalanine, BSH = borocaptate sodium.

Data management and statistics

Data collection, management and analyses were conducted by the independent datacenter in the Translational Research Center, Kyoto University Hospital. OS and PFS were analyzed using the Kaplan–Meier method. All statistical analyses were performed using SAS version 9.1.3 (SAS Institute Inc., Cary, NC, USA).

Table 2. Patient and tumor characteristics

	n
Total cases	62
Disease presentation	
Recurrent tumor	49
Newly diagnosed tumor	13
Gender	
Male	39
Female	23
Median age (range)	61 (31–85)
Treatment sites	
Oral cavity	24
Nasal cavity, Paranasal sinuses	17
Oropharynx	5
Larynx	1
Parotid gland	3
Temporal	2
Orbit	3
Mandible	3
Neck	10
Submental	1
Histology	
Squamous	33
Mucoepidermoid	5
Adenoidcystic	4
Acinic cell carcinoma	1
Polymorphous low-grade adenocarcinoma	1
Papillary cystadenocarcinoma	1
Malignant melanoma	11
Papillary adenocarcinoma	2
Inflammatory myofibroblastic tumor	1
Undifferenfiated carcinoma	1
Angiosarcoma	1
Osteosarcoma	1

RESULTS

Patient characteristics

Patient characteristics are detailed in Table 2. A total of 62 patients were treated with BNCT between December 2001 and September 2007. All the patients in this study had unresectable advanced or recurrent head and neck cancers. Of the 62, 13 (21%) patients had newly diagnosed unresectable tumors, and 49 (79%) patients had recurrent tumors. In the 49 patients, 41 (84%), 36 (73%) and 39 (80%) had undergone previous surgical resection, radiotherapy and chemotherapy, respectively. The majority of treatment sites were oral cavity, nasal cavity, paranasal sinuses, or neck. Patients with squamous cell carcinoma, adenocarcinoma and malignant melanoma numbered 33 (53%), 20 (32%) and 11 (18%), respectively.

Treatment characteristics

Treatment characteristics are summarized in Table 3. Of the 62 patients, 42 received BNCT once, 17 received it twice, two received it three times, and one received it five times. A total of 87 BNCT procedures were performed on the 62 patients. Both BSH and BPA-f were used in 13 treatments, and BPA-f alone was used in 72. In the 72 treatments with BPA-f alone, a dose of 250 mg/kg was used in five treatments and 500 mg/kg in 67.

The median tumor diameter and depth from the skin was 48 mm (range, 10–135 mm) and 50 mm (range, 0–100 mm),

Table 3. Treatment characteristics

Total BNCT treatments	**87**
Once	42 cases
Twice	17 cases
Three times	2 cases
Five times	1 case
Boron compound	
Both BSH and BPA	13
BPA alone	72
250 mg/kg	5
500 mg/kg	67
	Median (range)
Maximum tumor diameter (mm)	48 mm (10–135)
Maximum tumor depth (mm)	50 mm (0–100)
T/B ratio	3.0 (1.7–6.1)
Minimum tumor dose (Gy-eq)	17.9 (4.0–44.5)
Maximum skin dose (Gy-eq)	6.9 (2.7–30.3)
Maximum oral mucus dose (Gy-eq)	10.9 (4.4–17.2)

T/B ratio = tumor/blood ratio.

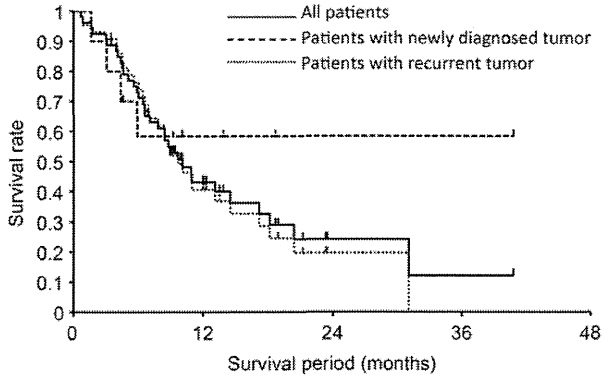

Fig. 1. OS for all patients, those with a newly diagnosed tumor, and those with a recurrent tumor.

respectively. The median T/B ratio assessed before BNCT by the ^{18}F-BPA PET study was 3.0 (range, 1.7–6.1). The median minimum tumor dose was 17.9 Gy-eq (range, 4.0–44.5 Gy-eq). The median maximum skin and oral mucosa doses were 6.9 Gy-eq (range, 2.7–30.3 Gy-eq) and 10.9 (range, 4.4–17.2 Gy-eq), respectively.

Treatment results

Survival data were available for 53 patients. The median follow-up was 18.7 months (range, 0.7–40.8 months). Response to BNCT was assessed using imaging studies, CT or MRI, performed within 6 months after BNCT. In 57 patients, the response data were valid. Of the 57, 16 patients (28%) showed a complete response (CR), and 17 patients (30%) had a partial response (PR). The overall response rate (CR + PR) for all the patients, the 13 patients with newly diagnosed unrespectable tumors and the 46 with recurrent tumors was 58%, 39% and 61% within 6 months after BNCT, respectively.

The median survival time (MST) was 10.1 months from the time of BNCT, and the 1- and 2-year OS rates were 43% and 24%, respectively (Fig. 1). The 1-year OS rate for the 10 patients with newly diagnosed unresectable tumors and the 43 with recurrent tumors was 58% and 41%, respectively (Fig. 1). In the patients with recurrent tumors, the MST, median PFS time and 1-year PFS rate were 9.7 months, 5.1 months and 5%, respectively. In the analysis of the patients with recurrent tumors, the 1-year OS rates for squamous cell carcinoma ($n = 29$), malignant melanoma ($n = 6$), and adenocarcinoma ($n = 6$) were 26%, 60% and 100%, respectively.

Toxicity

The acute adverse events occurring within 1 month after BNCT were analyzed because 43% of the patients underwent other therapies following BNCT. BNCT-related acute toxicities were graded according to the CTCAE v3.0 and are listed in Table 4. The major acute Grade 3 or 4 toxicities were hyperamylasemia (38.6%), fatigue (6.5%), mucositis/stomatitis (9.7%) and pain (9.7%), all of which were manageable. One of these toxicities, hyperamylasemia, was presumably the result of irradiation of the salivary gland. This was an inevitable adverse event but did not lead to any serious situation. Three patients experienced carotid artery hemorrhage, and two died of rupture of an infected carotid artery. In addition, the carotid arteries that ruptured were invaded by recurrent tumor and reirradiated with BNCT. One patient died from malnutrition secondary to poor feeding. Details of these four patients are presented in Table 5.

Table 4. Acute adverse events at 1 month after BNCT

Adverse event	Grade 3	Grade 4	% Grade 3/4
Anemia	0	1	1.6
Leucopenia	0	1	1.6
Thrombocytopenia	0	1	1.6
Hyperamylasemia	10	7	27.4
Renal toxicity	1	0	1.6
Hearing loss	2	0	3.2
Otitis, external ear (non-infectious)	0	1	1.6
Otitis, middle ear (non-infectious)	1	0	1.6
Fatigue	4	0	6.5
Radiation dermatitis	1	1	3.2
Ulceration (skin)	2	0	3.2
Xerostomia	1	0	1.6
Dysphagia	2	0	3.2
Mucositis	4	2	9.7
Keratitis	1	0	1.6
Pain	6	0	9.7
Dyspnea	3	0	4.8
Edema, larynx	2	0	3.2
Vocal changes	1	0	1.6

DISCUSSION

The purpose of this outcomes study was to investigate the safety and efficacy of BNCT for advanced or recurrent head and neck cancers. With regard to safety, the incidence of high-grade (≥3) toxicity, except for hyperamylasemia, was <10%. The incidence of Grade 3 and 4 acute dermatitis and mucositis/stomatitis was 3.2% and 9.7%, respectively, which was acceptably low considering that 79% patients with recurrent tumor received reirradiation with BNCT. A dose <10–12 Gy-eq for skin and oral mucosa was set as the dose constraint; therefore, the median maximum doses delivered

Table 5. Severe BNCT-related toxicities

Patient	Treatment site	Previous RT dose	Interval between BNCT and complication (months)	BNCT tumor dose	Toxicity
1	Lt. parotid	45 Gy	18.0	66.2 Gy-eq	Lt. carotid hemorrhage requiring salvage operation
2	Lt. mandible	80.2 Gy	6.0	28.9 Gy-eq	Malnutrition due to poor feeding; patient subsequently died
3	Lt. neck	66 Gy	2.0	25.3 Gy-eq	Lt. carotid hemorrhage; patient died
4	Larynx	60 Gy	4.5	33.7 Gy-eq	Rt. carotid hemorrhage; patient died

RT = Radiotherapy.

to the skin and mucosa were estimated at 6.9 and 10.9 Gy-eq, respectively (Table 2). The dose calculation for BNCT has more complexity and uncertainty compared with other radiotherapy modalities. For example, the CBE factor (photon-equivalent convergent coefficient) for skin is different from that for oral mucosa, and the ^{10}B concentration in normal tissues is assumed to be equal to that in the blood. Since, in this retrospective study, acute adverse effect was evaluated once at 1 month after BNCT, further prospective trials are needed for evaluation of late adverse effects. With regard to dose evaluation, acceptable acute skin and mucosa toxicity revealed in this present study suggests that the parameters and assumptions used in the BNCT dose calculation were appropriate and feasible.

One serious adverse reaction in the treatment of head and neck cancer with radiotherapy was carotid hemorrhage. This event occurred in three patients in the present study, and two of them died. The incidence rate of carotid hemorrhage (4.8%) observed in this study was comparable with that reported in the literature [9]. In all three cases, the ruptured carotid artery was invaded by the surrounding advanced tumor. Although BNCT can deposit a large dose gradient between the tumor and surrounding normal tissues, BNCT should be applied cautiously to such cases. If a carotid artery is surrounded by the tumor, angiography for evaluating the wall of the carotid artery should be performed. Irregularity of the wall suggests the invasion of the carotid artery by the surrounding tumor. BNCT should not be indicated in such cases.

The selected studies of concurrent reirradiation and chemotherapy for recurrent head and neck cancer are summarized in Table 6 [10–18]. According to these reports, concurrent chemo-reirradiation trials yielded an overall response rate ranging from 41–80%, MST 8.5–14 months, 1-year OS 37–56%, and 2-year OS 15–35%. The results in this study were difficult to compare with those in trials of chemo-irradiation as a result of the loss of survival data for 9 patients (15%), the heterogeneity of the patients and tumors, including different tumor status (recurrent or newly diagnosed), varying histology (squamous cell carcinoma, melanoma, adenocarcinoma, and others), and different chemotherapy after BNCT. However, the overall response rate and MST, and 1-year OS for recurrent head and neck cancer in the present study were 61%, 9.7 months and 41%, which are promising results and warrant a further prospective clinical trial of BNCT for recurrent head and neck cancer.

Recently, intensity-modulated radiotherapy (IMRT) and stereotactic radiotherapy (SRT), as forms of reirradiation, have been applied to the treatment of recurrent, previously irradiated head and neck cancer. These techniques can deliver a definitive dose to the recurrent tumor while sparing neighboring normal tissues. Sulman *et al.* have reported the results of a study in which all 78 patients were treated with IMRT. The 2-year OS and local control rates were 58% and 64%, respectively [19]. Roh *et al.* have reported their

Table 6: Treatment outcomes of chemo-reirradiation for recurrent head and neck cancer

Authors	*n*	Radiotherapy	Chemotherapy	Response rate	Survival
De Crevoisier *et al.* [10]	169	Median 60 Gy	HU, 5-FU or MMC, 5-FU, CDDP	CR: 37%	2-year OS: 21%
				PR: 11%	
Langer *et al.* [11]	99	60 Gy: 1.5 Gy b.i.d.	CDDP, paclitaxel	Not mentioned	MST: 12.1 months
					1-year OS: 50.2%
					2-year OS: 25.9%
Spencer *et al.* [12]	52	Median 50 Gy	5-FU, HU	CR: 30%	MST: 9.4 months
				PR: 22%	1-year OS: 39%
					2-year OS: 15%
Spencer *et al.* [13]	79	60 Gy: 1.5 Gy b.i.d.	5-FU, HU	Not mentioned	MST: 8.5 months
					1-year OS: 40.5%
					2-year OS: 15.2%
Schaefer *et al.* [14]	32	Median 50 Gy	5-FU, HU	CR: 19%	MST: 9.0 months
				PR: 22%	1-year OS: 39%
Weppelmann *et al.* [15]	21	40 Gy ($n = 11$)	5FU, HU	CR: 43%	1-year OS: 56%
		48 Gy ($n = 10$)		PR: 29%	
Kramer *et al.* [16]	34	60 Gy: 1.5 Gy b.i.d.	CDDP, paclitaxel	Not mentioned	MST: 12.4 months
					1-year OS: 50%
					2-year OS: 35%
Hehr *et al.* [17]	27	40 Gy	CDDP, dicotaxel	CR: 36%	MST: 10 months
				PR: 44%	1-year OS: 37%
					3-year OS: 18%
Cohen *et al.* [18]	25	72 Gy	CDDP, tirapazamine	CR: 28%	MST: 14 months
				PR: 20%	1-year OS: 56%
					2-year OS: 27%

HU = hydroxyuria, 5-FU = 5-fluorouracil, CR = complete response, PR = partial response, OS = overall survival, b.i.d. = twice daily, CDDP = cisplatine, MST = median survival time.

experience of SRT using CyberKnife for recurrent head and neck cancer [20]. The response rate (CR + PR) was 80%, and the 1- and 2-year OS rates were 52.1% and 30.9%, respectively. In both studies, local control and survival data were superior to those obtained with concurrent chemo-reirradiation using conventional irradiation techniques, and treatment-related morbidity was less common. Therefore, reirradiation using these new techniques has the potential to become standard therapy for locally recurrent head and neck cancer.

In these circumstances of remarkable progress in radiotherapy techniques, we have investigated the possibility that BNCT can be applied to locally advanced or recurrent head and neck cancer. The drawback of BNCT is that deep-seated tumors cannot receive an sufficient irradiation dosethe owing to poor penetration of thermal neutrons in the body. In the present study, the maximum tumor depth ranged from 0–100 mm, and the minimum tumor dose ranged from 4.0–44.5 Gy-eq, which indicates that, in many cases, the doses delivered to the deep-seated tumors were insufficient to control the tumors. In addition, we calculated the tumor dose on the assumption that BPA distributed homogeneously in the tumor. The region with insufficient distribution of BPA may receive much a lower dose compared with the calculated minimum tumor dose. Therefore, in future clinical trials, BNCT for head and neck cancer should be limited to shallow-seated tumors, and the dose constraint should be set to the dose delivered to normal mucosa or skin in which BPA is assumed to distribute more homogeneously compared with the tumor.

All the patients with adenocarcinoma survived, although the number was very small. ^{4}He particles and ^{7}Li nuclei irradiating the tumor in BNCT are high-LET heavy ion particles; therefore, BNCT is theoretically expected to control radioresistant tumors such as adenocarcinoma. In addition, adenocarcinoma in the head and neck region has a tendency

for microscopic perineural invasion. In IMRT or SRT for recurrent head and neck cancer, the planning target volume (PTV) margin is commonly very small (0–5 mm); therefore, microscopic perineural invasion has the risk of extending out of the PTV. In contrast, in BNCT, neutron beams irradiate the tumor with a wide margin >5 cm, using a 10–15-cm diameter round collimator. Therefore, BNCT has the potential to eradicate cancer cells that microscopically invade the tumor and exist in the perineural portion outside the gross tumor. Adenocarcinoma is a good indication for BNCT, especially when at a shallow location.

CONCLUSION

In conclusion, this study of BNCT for advanced or recurrent tumors revealed two important findings. First, we confirmed the feasibility of our dose-evaluation method with regard to skin and oral mucosa. Second BNCT-related morbidity and mortality were acceptably low. This study warrants the clinical trial in the planning stage with full consideration of the eligibility criteria, especially in regard to the maximum tumor depth and histology.

ACKNOWLEDGEMENTS

We are indebted to Prof. Akira Shimizu for designing this study.

REFERENCES

1. Haraf DJ, Weichselbaum RR, Vokes EE. Reirradiation with concomitant chemotherapy of unresectable recurrent head and neck cancer: a potentially curable disease. *Ann Oncol* 1996;**7**:913–8.
2. Spencer SA, Harris J, Wheeler RH *et al.* Final report of RTOG 9610, a multi-institutional trial of reirradiation and chemotherapy for unresectable recurrent squamous cell carcinoma of the head and neck. *Head Neck* 2008;**30**:281–8.
3. Coderre JA, Morris GM. The radiation biology of boron neutron capture therapy. *Radiat Res* 1999;**151**:1–18.
4. Kato I, Ono K, Sakurai Y *et al.* Effectiveness of BNCT for recurrent head and neck malignancies. *Appl Radiat Isot* 2004;**61**:1069–73.
5. Kankaanranta L, Seppälä T, Koivunoro H *et al.* Boron neutron capture therapy in the treatment of locally recurred head-and-neck cancer: final analysis of a phase I/II trial. *Int J Radiat Oncol Biol Phys* 2012;**82**:e67–75.
6. Aihara T, Hiratsuka J, Morita N *et al.* First clinical case of boron neutron capture therapy for head and neck malignancies using 18F-BPA PET. *Head Neck* 2006;**28**:850–5.
7. Nigg DW, Wemple CA, Wessol DE *et al.* SERA—an advanced treatment planning system for neutron capture therapy and BNCT. *Trans Am Nucl Soc* 1999;**80**:66–8.
8. Suzuki M, Sakurai Y, Masunaga S *et al.* Dosimetric study of boron neutron capture therapy with borocaptate sodium (BSH)/lipiodol emulsion (BSH/lipiodol-BNCT) for treatment of multiple liver tumors. *Int J Radiat Oncol Biol Phys* 2004; **58**:892–6.
9. Salama JK, Vokes EE, Chmura SJ *et al.* Long-term outcome of concurrent chemotherapy and reirradiation for recurrent and second primary head-and-neck squamous cell carcinoma. *Int J Radiat Oncol Biol Phys* 2006;**64**:382–91.
10. De Crevoisier R, Bourhis J, Domenge C *et al.* Full-dose reirradiation for unresectable head and neck carcinoma: experience at the Gustave-Roussy Institute in a series of 169 patients. *J Clin Oncol* 1998;**16**:3556–62.
11. Langer CJ, Harris J, Horwitz EM *et al.* Phase II study of low-dose paclitaxel and cisplatin in combination with split-course concomitant twice-daily reirradiation in recurrent squamous cell carcinoma of the head and neck: results of Radiation Therapy Oncology Group Protocol 9911. *J Clin Oncol* 2007;**25**:4800–5.
12. Spencer SA, Wheeler R, Peters G *et al.* Phase 1 trial of combined chemotherapy and reirradiation for recurrent unresectable head and neck cancer. *Head Neck* 2003;**25**: 118–22.
13. Spencer SA, Harris J, Wheeler RH *et al.* Final report of RTOG 9610, a multi-institutional trial of reirradiation and chemotherapy for unresectable recurrent squamous cell carcinoma of the head and neck. *Head Neck* 2008;**30**:281–8.
14. Schaefer U, Micke O, Schueller P *et al.* Recurrent head and neck cancer: retreatment of previously irradiated areas with combined chemotherapy and radiation therapy – results of a prospective study. Radiology 2000;**216**:371–6.
15. Weppelmann B, Wheeler RH, Peters GE *et al.* Treatment of recurrent head and neck cancer with 5-fluorouracil, hydroxyurea, and reirradiation. *Int J Radiat Oncol Biol Phys* 1992;**22**: 1051–6.
16. Kramer NM, Horwitz EM, Cheng J *et al.* Toxicity and outcome analysis of patients with recurrent head and neck cancer treated with hyperfractionated split-course reirradiation and concurrent cisplatin and paclitaxel chemotherapy from two prospective phase I and II studies. *Head Neck* 2005;**27**:406–14.
17. Hehr T, Classen J, Belka C *et al.* Reirradiation alternating with docetaxel and cisplatin in inoperable recurrence of head-and-neck cancer: a prospective phase I/II trial. *Int J Radiat Oncol Biol Phys* 2005;**61**:1423–31.
18. Cohen EE, Rosine D, Haraf DJ *et al.* Phase I trial of tirapazamine, cisplatin, and concurrent accelerated boost reirradiation in patients with recurrent head and neck cancer. *Int J Radiat Oncol Biol Phys* 2007;**67**:678–84.
19. Sulman EP, Schwartz DL, Le TT *et al.* IMRT reirradiation of head and neck cancer-disease control and morbidity outcomes. *Int J Radiat Oncol Biol Phys* 2009;**73**:399–409.
20. Roh KW, Jang JS, Kim MS *et al.* Fractionated stereotactic radiotherapy as reirradiation for locally recurrent head and neck cancer. *Int J Radiat Oncol Biol Phys* 2009;**74**:1348–55.

ANTICANCER RESEARCH *34*: 3759-3764 (2014)

Docetaxel/ TS-1 with Radiation for Unresectable Squamous Cell Carcinoma of the Esophagus - A Phase II Trial

HIDEO MATSUMOTO[1], HISAKO KUBOTA[1], MASAHARU HIGASHIDA[1], EISAKU YODEN[2], JUNICHI HIRATSUKA[2], KEN HARUMA[3], MASAFUMI NAKAMURA[1] and TOSHIHIRO HIRAI[1]

Departments of [1]Digestive Surgery, [2]Radiology and [3]Gastroenterological Medicine, Kawasaki Medical School, Kurashiki City, Okayama, Japan

Abstract. *Background: We tried a new regimen of docetaxel / TS-1 (tegafur-gimestat-otastat potassium) combined with radiation for squamous cell carcinoma of the esophagus in a phase II trial. Patients and Methods: The patients, whose tumor invaded other organs without other organ metastasis, were given TS-1 (60 mg/m^2/day) from days 1 to 14, and docetaxel (20-30 mg/m^2) on days 1 and 8. They received radiation in 2.0 Gy from days 1 to 21. Patients were given a seven-day rest after the first course, and then were treated with the same regimen from days 28 to 49. Results: Seventeen cases were enrolled in the study. The response rate was 76.4% (13/17). The overall 5-year survival rate was 29.6% (5/17) and median survival time was 15.2 months. Adverse events more than grade 3 occurred in 10 cases. Conclusion: This combination therapy may be one of the most effective treatments because of its lower rate of non-hematological adverse events and higher response rate. Three cases also underwent salvage surgery when the tumor recurred, and in one case, chemoradiation to a metastatic nodule on the thoracic wall was added.*

Esophageal cancer is the sixth-most common cause of cancer-related death worldwide (1). Although significant improvements have been achieved in both the diagnosis, and treatment of patients with esophageal cancer, their prognosis remains poor, with 5-year survival of 17% during the period 1996-2004 (2).

Surgery might be a most effective treatment for patients with esophageal cancer. However, chemoradiotherapy is another effective therapy when curative resection is difficult because of advanced stage invading to other organs.

Correspondence to: Hideo Matsumoto, MD, Ph.D., Department of Digestive Surgery, Kawasaki Medical School, 577 Matsushima, Kurashiki City, Okayama, 701-0192, Japan. Tel: +81 864621111, Fax: +81 864621199, e-mail: h-matsu@med.kawasaki-m.ac.jp

Key Words: Docetaxel, TS-1, chemoradiation, unresectable squamous cell carcinoma of esophagus.

Chemoradiotherapy has been reported to significantly increase the survival rate of patients with esophageal cancer (3, 4). The standard regimen of the chemoradiation has consisted of 5-fluorouracil (5-FU) and cisplatin concomitant with 50-60 Gy radiation for over 20 years from the 1990s. This regimen is effective and safe, but needs hospitalization as it requires a large amount of hydration and for the control of the severe digestive symptoms; *e.g.* nausea, and appetite loss.

We tried a combination regimen consisting of docetaxel and TS-1 (a drug comprising tegafur, gimeracil and oteracil) concomitant with radiation to assess the possibility of achieving the same efficacy without hospitalization and with reduction of severe digestive symptoms.

Docetaxel has been extensively used with radiation for the treatment of patients with non-small cell lung cancer and head and neck cancer (5, 6). Docetaxel is a novel semi-synthetic taxane and has been shown to enhance response to radiation, with induced mitotic arrest and apoptosis in murine tumor cells (7, 8).

TS-1 was introduced as a novel oral anticancer drug. TS-1 is now considered to be a key treatment modality in the control of head and neck cancer (8, 9) and advanced gastric cancer (10, 11) in Japan. Moreover, it has recently been reported that gimeracil might enhance the efficacy of radiotherapy through suppression of homologous recombination-mediated DNA repair pathways (12, 13).

This combination of docetaxel and TS-1 has been demonstrated to have a synergistic effect which was explained by biochemical modulation of the expression of thymidine synthetase, dihydropyrimidine dehydrogenase, and orotate phosphorybosyl transferase, the components of TS-1 (14, 15). This combination has a synergistic effect on cancer in addition to the radio sensitizing and cytotoxic effect of each drug.

For these reasons, we started this study in 2006 at a single Institute. The recommended dose of docetaxel was determined by dose-escalation phase I study as 30mg/m^2 (16). The degree of dose-escalation was level 3. TS-1 was fixed at 60 mg/m^2.

0250-7005/2014 $2.00+.40

However, we reduced the dose of docetaxel from 30 mg/m^2 to 20 mg/m^2 according to the recommendation of the Safety Review Committee due to treatment-related death in March, 2010, because it was considered that the dose of level 1 was sufficiently effective for reducing the occurrence of pneumonitis. Three patients were treated at the decreased dose.

Patients and Methods

Eligibility was as follows: The patients were required to have histologically-proven squamous cell carcinoma of the esophagus. The tumor was T4 without other organ metastasis or recurrent cancer. The tumor was a measurable lesion. All areas of the disease were to be encompassed in the radiation port. The patient's Eastern Cooperative Oncology Group (ECOG) performance status had to be 0 to 1. The patient's age was over 20 and under 80 years. Life expectancy was more than 12 weeks. Patients with esophagobronchial fistulas were excluded. Adequate organ function was required: adequate bone marrow function (hemoglobin level >9.5 g/dl, white blood cell count >4,000 mm^3, neutrophil count >2,000/mm^3 and platelet count >100,000/mm^3), adequate hepatic function (total bilirubin level <1.5 mg/dl, asparate aminotransferase and alanine aminotransferase levels <2× the upper limit of normal), adequate renal function (serum creatinin level <1.5 mg/dl). Patients were required to have no other active cancer. The patients provided their written informed consent to receive this chemoradiotherapy at our Hospital.

Seventeen patients were enrolled from April, 2006 to December 2012. In this period, 230 patients with esophageal cancer were treated at our hospital. One hundred and forty-five patients underwent esophagectomy and 55 patients were treated by chemoradiation.

Patients were given TS-1 (60 mg/m^2/day) orally from days 1 to 14, and Docetaxel (20-30 mg/m^2) intravenously on days 1 and 8. Megavoltage radiotherapy was performed with standard fractionation (1.8-2.0 Gy per fraction, five days per week) concurrently with chemotherapy. Patients were given a one-week rest at the fourth week, and then treated with the same regimen from day 29. Radiation fields included gross tumor volumes (primary tumor and involved lymph nodes) and regional lymph nodes (supraclavicular and mediastinal nodes) with adequate margins in all patients. Prescribed dose to gross tumor volumes was aimed at 60 Gy. When the prescription dose conflicted with normal tissue tolerance, altered prescription dose of 54 Gy (in five patients) or 50.4 Gy (in two patients) was applied.

The primary end-point was overall response and secondary endpoints were overall survival, progression-free survival, local control rate and toxicities.

All patients were evaluated every one to two months. The effect of therapy was assessed using the Response Evaluation Criteria in Solid Tumors (RECIST v 1.1) (17). Adverse events were assessed using the Common Terminology Criteria for Adverse Events (CTCAE v 4.0) (18).

TS-1 has not yet received approval for esophageal cancer in Japan but this study was approved by the Institutional Review Board of Kawasaki Medical School (approval No.204, 204-1).

Statistical analysis. Overall survival was measured from the treatment start date to the date of the patient's death. Time-to-progression (TTP) was measured from the start of treatment to the date of estimated progression according to RECIST. The Kaplan Meier method was used to estimate the overall survival time. Estimated survival times were based on the confirmation date of final survival. Statistical calculations were performed with the JMP® 8 statistical software produced by SAS Institute Inc. (Cary, NC, USA).

Table I. *Patients' characteristics.*

Characteristics		n=17
Gender	Male	15
	Female	2
Age, years	Median	64±8.5
	Range	40-79
Target lesion		
	Esophagus	16
	Cervical lymph node	11
	Mediastinal lymph node	1
T4 organ	Trachea	12
	Aorta	8

Results

Of the 17 measurable cases, 15 patients were males and two patients were females. Their median age was 64 (range 40-79) years old. Target lesions were esophagus in 16 cases, cervical lymph nodes in 11 cases, mediastinal lymph nodes in one case. T4 organs were trachea in 10 cases, aorta in 8 cases (Table I). Some cases were included more than once due to the presence of more than one lesion.

There were three CR, 10 showed PR, one showed SD and three showed PD. The response rate was 76.4% (13/17) and disease control rate was 82.4% (14/17). Four patients underwent salvage esophagectomy and one patient underwent additional chemoradiation for a metastatic pleural nodule of docetaxel/nedaplatin with RT (19). Five-year overall survival was 29.6% (5/17) and the median overall survival time was 15.2 months (Figure 1). Five-year progression-free survival rate of the effectively-treated patients was 41.4% (5/14) and the median progression-free survival time was 26.8 months (Figure 2).

Unfortunately, one case suffered treatment-related death due to cytomegalovirus infection followed by grade 4 pneumonitis. Major toxicities included myelosuppression and esophagitis. Most toxicities were grade 3 or less (Table II). One patient was treated as an outpatient using this regimen.

Discussion

Chemoradiotherapy using docetaxel plus TS-1 concomitant radiation led to a high response rate and high survival rate. In this regimen, patients were free from the need for large amounts of hydration and continuous infusion of anti-cancer drug.